IEEE Access
Multidisciplinary | Rapid Review | Open Access Journal

Received July 16, 2019, accepted August 1, 2019, date of publication August 12, 2019, date of current version August 26, 2019.

*Digital Object Identifier 10.1109/ACCESS.2019.2934506*

# A Broadband Balun With Complex Impedance Transformation and High Isolation

**ERIC S. LI[1], CHIN-TSE LIN[1], HUAYAN JIN[2], AND KUO-SHENG CHIN[3], (Senior Member, IEEE)**

[1]Department of Electronic Engineering, National Taipei University of Technology, Taipei 10608, Taiwan
[2]Key Laboratory of RF Circuits and System of Ministry of Education, Institute of Antennas and Microwave Technology, Hangzhou Dianzi University, Hangzhou 310018, China
[3]Department of Electronic Engineering, Chang Gung University, Taoyuan 333, Taiwan

Corresponding author: Kuo-Sheng Chin (kschin@mail.cgu.edu.tw)

This work was supported in part by the Ministry of Science and Technology under Grant MOST 108-2221-E-182-002, and in part by the Chang Gung University, Taiwan, under Grant BMRP 903.

**ABSTRACT** The design of baluns with wide bandwidth, transformation between complex source and load impedances, and high isolation is presented in this paper. These features can be accomplished simultaneously by employing double-stub couple lines (DSCL). The differential characteristics are established by only exciting the odd-mode operation of the balun, and suppressing its even-mode operation. For the odd-mode operation, the structure of the DSCL acts as a multi-stub structure and contributes to bandwidth enhancement. An additional resistor added to the DSCL between the output ports improves their isolation and contributes to the impedance transformation. An experiment was prepared for the operations of the proposed design at 2.8 GHz with $Z_S = 35 - j10\ \Omega$ and $Z_L = 60 + j10\ \Omega$. A measured wide bandwidth of 35% was obtained under the criterions of $|S_{11}| < -10$ dB, $(\angle S_{31} - \angle S_{21}) < 180^\circ \pm 5^\circ$, and $(|S_{31}| - |S_{21}|) < 1$ dB.

**INDEX TERMS** Broadband balun, coupled line, high isolation, complex impedance transformation.

## I. INTRODUCTION

In recent years, more and more professionals have chosen differential-in designs for wireless circuits because the designs provide the advantages of immunity to noises and interferences. The differential signals can be generated through baluns, which convert a single-ended unbalanced signal into two differential-in balanced signals. Many applications require baluns with advanced functions such as compact size, broadband or multi-band operations, real or complex impedance transformations, high isolation, and filtering characteristics, which has initiated a great deal of research activities on topics related to advanced baluns.

There have been quite a few designs for advanced baluns from recent publications [1]–[16]. In [1], a branch-line coupler with an open isolated port can provide differential signals by connecting an open stub to the middle of each lateral transmission line. The balun can conduct impedance transformation, but lacks isolation. A dual-band balun was constructed by four pairs of parallel coupled lines and six open stubs [2], which can offer the function of impedance transformation. However, the conversion is only applicable to real impedances. In [3], the combination of three pairs of coupled lines, two open stubs, and resistors produces a compact balun capable of transforming complex impedances. A lumped balun with complex impedance transformation was designed based on an asymmetric modification of the out-of-phase-compensated power splitter topology [4]. However, the lumped elements fail to function properly at higher frequencies. In [5], the function of tunable power division ratio was achieved by modifying the conventional Marchand balun with a varactor and a resistor added to the middle of two pairs of coupled lines. A Marchand balun with open-circuited ends and a capacitive feeding can reduce its length to around 1/3 compared with the conventional design [6]. The stacked composite resonators [7] and coupled half-wavelength microstrip resonators [8], were developed for designs of filtering baluns. The designs explored in [9], [10] are based on the Wilkinson power dividers. The property of 180° phase shift between two output signals is achieved by replacing one of the λ/4 transmission lines with a 3λ/4 line or its substitutes. The designs can achieve high isolation.

As to bandwidth enhancement, multi-section designs would produce more bandwidth, but the prices are large size and the need for high-impedance lines. In [11], a broadband

The associate editor coordinating the review of this article and approving it for publication was Lei Zhao.

balun with vertical transition between conductor-backed coplanar waveguide and parallel-strip transmission line was presented. In [12], a broadband balun constructed from a broadband phase inverter presented in parallel strips and a broadband impedance matching network with short-circuited stubs was demonstrated. A planar balun consisting of a broadband Wilkinson power divider and a noncoupled-line broadband 180° phase shifter was developed in [13]. In [14], a new design methodology was presented to improve the bandwidth of a Marchand balun. In [15], a balun based on an artificial fractal-shaped composite right/left-handed transmission line was developed for bandwidth enhancement and size reduction. In [16], a lumped-element balun developed from an asymmetrical four-port network with a tail inductor was proposed. All those broadband baluns [11]–[16] do not possess function of impedance transformation.

As shown above, the advanced baluns can be improved in three aspects. First, the bandwidth enhancement of baluns is important for broadband communication applications. Second, the balun featuring complex impedance transformation can significantly reduce system size due to the direct connection between the balun and the complex ports of external devices. Third, the balun with high isolation plays an important role in the balance circuits to prevent signal interference.

To achieve these three design goals simultaneously, a balun featuring wide bandwidth, transformation of complex impedances, and high isolation is proposed in this paper. The double-stub couple line (DSCL) is applied to the balun. By suppressing its even-mode operations, the odd-mode operations lead the two outputs out of phase by 180°. For the odd-mode operation, the structure of the DSCL acts as a multi-stub structure and contributes to bandwidth enhancement. An isolation resistor introduced between the output ports further establishes the function of transformation of complex impedances and the property of high isolation. The details of this design are disclosed in the follow-up sections. Section II provides the analysis for the broadband balun featuring transformation of complex impedances and high isolation. The experimental verification and discussion are presented in Section III. The results show superior performance on complex impedance transformation, high isolation, and wide bandwidth. At the end, a conclusion for this study is prepared.

## II. BROADBAND BALUN FEATURING TRANSFORMATION BETWEEN A COMPLEX SOURCE AND A COMPLEX LOAD IMPEDANCES

In this section, a balun is developed for broadband applications, which is also capable of conducting transformation between a complex source and a complex load impedances. The broadband property of the proposed design is contributed by the DSCL shown in Fig. 1, which is derived from a λ/4 transmission line, as described in [17]. The DSCL consists of a main transmission line ($Z_A$, $\theta_A$) and a parallel

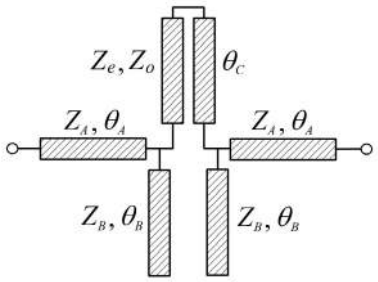


**FIGURE 1.** The circuit model for the double-stub coupled line (DSCL).

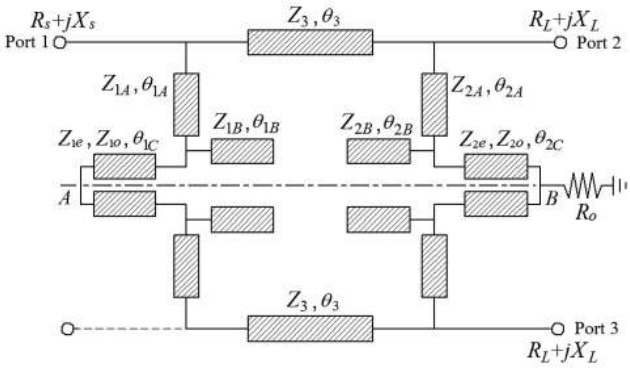


**FIGURE 2.** The circuit model for the proposed balun using the DSCLs.

coupled line ($Z_e$, $Z_o$, $\theta_C$) connected to the middle of the main line. The two lines of the coupled line are short to each other at one end, and are connected to two open stubs ($Z_B$, $\theta_B$), respectively, and the main line at the other end. Fig. 2 illustrates the circuit model for the proposed balun, in which the DSCLs are used to replace the lateral λ/4 transmission lines of a branch-line coupler to establish a broadband balun. The design parameters of the DSCL can be managed to only allow its odd-mode operation, and to suppress its even-mode operation to obtain differential output signals. For the odd-mode operation, the structure of the DSCL is reduced to a stepped-impedance line short to ground at one end and tapped with an open stub in the middle, which acts as a multi-stub structure and contributes to bandwidth enhancement. Note that the proposed DSCL is introduced for a broadband balun featuring complex impedance transformation and high isolation, which differs from the design in [17].

### A. EVEN-ODD MODE ANALYSIS

A three-port balun can be implemented by a four-port branch-line coupler with its isolated port left open, as shown in Fig. 2. The advantage of this coupler is its symmetric structure, which allows the application of even- and odd-mode analysis to meet the requirements of broadband property and phase different of 180° between the output ports. In addition, since a three-port device cannot serve as a lossless and reciprocal network with impedance matched at all ports simultaneously,

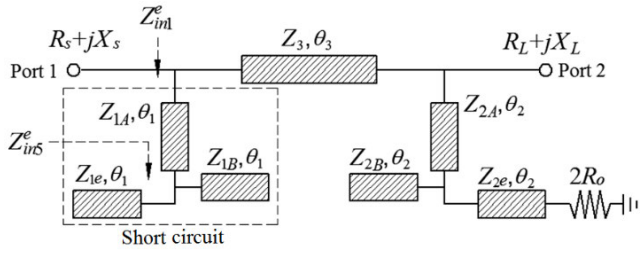


**FIGURE 3.** The even-mode circuit model for proposed balun.

a resistor is introduced between the output ports to achieve the performance of high output isolation, impedance matched at all three ports, and transformation of complex impedances. For a balun featuring above properties, its $S$ parameters must comply with the following conditions:

$$S_{ii} = 0, \quad \text{for } i = 1, 2, \text{ and } 3, \tag{1a}$$

$$S_{23} = 0, \tag{1b}$$

$$S_{21} = -S_{31}. \tag{1c}$$

One way to achieve the phase difference of 180° specified in (1c) for a balun design is to disable its even-mode transmission and to preserve its odd-mode operation. The former gives the following:

$$S^e_{21} = 0. \tag{2}$$

Further derivations would lead to the crucial equations below for the even- and odd-mode analysis on the balun[2],

$$S^e_{22} = 0, \tag{3a}$$

$$S^e_{11} + S^o_{11} - 2S^e_{11}S^o_{11} = 0, \tag{3b}$$

where the superscripts $e$ and $o$ represent even- and odd-modes, respectively. The even-mode circuit model of the proposed balun can be obtained from the circuit model given in Fig. 2 with the central dashed line section $A - B$ as a decoupling line, and is shown in Fig. 3. At its even-mode excitation, the left DSCL is required to be a short circuit, and the right DSCL becomes an open-circuited stepped-impedance line ($Z_{2A}$, $Z_{2B}$, $\theta_2$) tapped with a series connection of a stub ($Z_{2e}$, $\theta_2$) and a resistor $2R_o$. The circuit serves as an equivalent complex load to achieve impedance matching and high isolation.

To simplify the circuit design, the electrical lengths, $\theta_{1A}$, $\theta_{1B}$, $\theta_{1C}$, are set to be $\theta_1$; $\theta_{2A}$, $\theta_{2B}$, and $\theta_{2C}$ are equal to $\theta_2$; $\theta_3$ is fixed at 90°. The even-mode input impedance in Fig. 3, $Z^e_{in1}$, can be derived as

$$Z^e_{in1} = Z_{1A}\frac{Z^e_{in5} + jZ_{1A}\tan\theta_1}{Z_{1A} + jZ^e_{in5}\tan\theta_1}, \tag{4a}$$

$$Z^e_{in5} = -j\frac{Z_{1e}Z_{1B}\cot\theta_1}{Z_{1e}+Z_{1B}}. \tag{4b}$$

$Z^e_{in1}$ is set to be zero to satisfy the requirement noted in (2). The even-mode impedance of the coupled line, $Z_{1e}$, can be

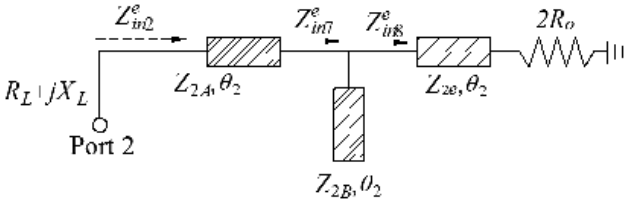


**FIGURE 4.** The reduced even-mode circuit model with Port 1 short to ground.

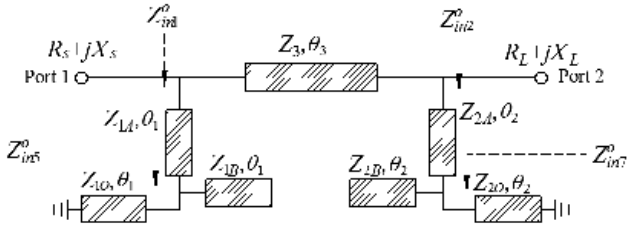


**FIGURE 5.** The odd-mode circuit model for the proposed balun.

obtained from the equations above, and is given by

$$Z_{1e} = \frac{Z_{1A}Z_{1B}\tan\theta_1}{Z_{1B}\cot\theta_1 - Z_{1A}\tan\theta_1}. \tag{5}$$

At the even-mode operation, Port 1 can be considered short to ground since $Z^e_{in1} = 0$. The associated reflection coefficient at Port 1, $S^e_{11}$, is given below according to [18],

$$S^e_{11} = \frac{-R_S + jX_S}{R_S + jX_S}. \tag{6}$$

The even-mode circuit model in Fig. 3 can be reduced to the one shown in Fig. 4. Based on the condition given in (3a), the even-mode input impedance at port 2, $Z^e_{in2}$, can be obtained as

$$Z^e_{in2} = R_L - jX_L. \tag{7}$$

The same impedance can be expressed in terms of the circuit elements in Fig. 4, and is given by

$$Z^e_{in2} = Z_{2A}\frac{Z^e_{in7} + jZ_{2A}\tan\theta_2}{Z_{2A} + jZ^e_{in7}\tan\theta_2}, \tag{8a}$$

$$Z^e_{in7} = \frac{Z^e_{in8}Z_{2B}\cot\theta_2}{Z_{2B}\cot\theta_2 + jZ^e_{in8}}, \tag{8b}$$

$$Z^e_{in8} = Z_{2e}\frac{2R_o + jZ_{2e}\tan\theta_2}{Z_{2e} + j2R_o\tan\theta_2}. \tag{8c}$$

The combination of (7) and (8) leads to solutions for $Z_{2e}$ and $R_o$, from which $Z_{2e}$ and $R_o$ become a function of $R_L$, $X_L$, $Z_{2A}$, $Z_{2B}$, and $\theta_2$. A root searching program is applied to simplify the process to determine $Z_{2e}$ and $R_o$.

Solutions for the odd-mode impedances $Z_{1o}$ and $Z_{2o}$ are treated differently. Fig. 5 shows the odd-mode circuit model

for the proposed broadband balun. The *ABCD* matrix of the odd-mode circuit model can be derived as

$$\begin{bmatrix} A_o & B_o \\ C_o & D_o \end{bmatrix} = \begin{bmatrix} 1 & 0 \\ \dfrac{1}{Z^o_{in1}} & 1 \end{bmatrix} \cdot \begin{bmatrix} \cos\theta_3 & jZ_3\sin\theta_3 \\ j\dfrac{\sin\theta_3}{Z_3} & \cos\theta_3 \end{bmatrix} \cdot \begin{bmatrix} 1 & 0 \\ \dfrac{1}{Z^o_{in2}} & 1 \end{bmatrix} = \begin{bmatrix} j\dfrac{Z_3}{Z^o_{in2}} & jZ_3 \\ j(\dfrac{1}{Z_3}+\dfrac{Z_3}{Z^o_{in1}Z^o_{in2}}) & j\dfrac{Z_3}{Z^o_{in1}} \end{bmatrix}_{\theta_3=90^o} \tag{9}$$

where $Z^o_{in1}$ and $Z^o_{in2}$ are the input impedances of the odd-mode circuit models for the DSCLs near Port 1 and Port 2, respectively, and are given by

$$Z^o_{in1} = Z_{1A}\frac{Z^o_{in5} + jZ_{1A}\tan\theta_1}{Z_{1A} + jZ^o_{in5}\tan\theta_1}, \tag{10a}$$

$$Z^o_{in2} = Z_{2A}\frac{Z^o_{in7} + jZ_{2A}\tan\theta_2}{Z_{2A} + jZ^o_{in7}\tan\theta_2}, \tag{10b}$$

$$Z^o_{in5} = \frac{jZ_{1B}Z_{1o}}{Z_{1B}\cot\theta_1 - Z_{1o}\tan\theta_1}, \tag{10c}$$

$$Z^o_{in7} = \frac{jZ_{2B}Z_{2o}}{Z_{2B}\cot\theta_2 - Z_{2o}\tan\theta_2}. \tag{10d}$$

The odd-mode reflection coefficient, $S^o_{11}$, can be expressed as

$$S^o_{11} = \frac{A_o(R_L+jX_L)+B_o-C_o(R_S-jX_S)(R_L+jX_L)-D_o(R_S-jX_S)}{A_o(R_L+jX_L)+B_o+C_o(R_S+jX_S)(R_L+jX_L)+D_o(R_S+jX_S)} \tag{11}$$

The solutions for the odd-mode impedances, $Z_{1o}$ and $Z_{2o}$, can be obtained by applying (6) and (9)–(11) into (3b), and their values can be determined through a root searching numerical technique.

### B. PARAMETRIC ANALYSIS

Both even- and odd-mode circuit models are $\pi$ networks with each of their lateral circuits characterized by a stepped-impedance stub tapped with an open-circuited stub in the middle, which would enhance the bandwidth of the balun. The line width and spacing of coupled lines are determined by the values of even- and odd-mode impedances. From the derivation above, the number of design equations is far less than the number of the circuit parameters of the balun. Thus, more choices are offered for the circuit dimensions. This under-determined feature is beneficial to circuit implementation since both line width and spacing of coupled lines are subject to the fabrication limits of PCBs.

The values of the even- and odd-mode impedances of the DSCLs can be determined by conducting a parametric study to observe the variations of $Z_{1e}$, $Z_{1o}$, $Z_{2e}$, and $Z_{2o}$ subject to the changes in $\theta_1$ and $\theta_2$, with other parameters fixed at some values. It can be seen from (5), (7), and (8), that $Z_{1e}$ is mainly influenced by the design parameters of the left DSCL; while $Z_{2e}$ is primarily affected by those of the right DSCL. The impedances $Z_{1o}$ and $Z_{2o}$ exhibit similar dependence as their individual paired impedances $Z_{1e}$ and $Z_{2e}$ do because even- and odd-mode impedances are together to determine the properties of a coupled line. The analysis would be easier if the design parameters of the two DSCLs are treated separately.

To simplify the parametric analysis of the even- and odd-mode impedances, the initial values of $Z_{1A}$, $Z_{1B}$, $Z_{2A}$, $Z_{2B}$, and $Z_3$ are confined to the numbers specified by sixteen impedance sets (Sets A–P) listed in Table 1. The electrical lengths $\theta_1$ and $\theta_2$ are chosen to be the variables for the analysis. Two combinations of source and load impedances are considered in this work. The pair of $Z_S = 35 - j10\ \Omega$ and $Z_L = 60 + j10\ \Omega$ is denoted by Case I, and the other pair of $Z_S = 40 - j90\ \Omega$ and $Z_L = 70 + j100\ \Omega$ is Case II.

Following the impedance values from Sets A–D, Fig. 6 shows the variations of $Z_{1e}$ and $Z_{1o}$ of the left DSCL subject to the changes in $\theta_1$ for Case I. As indicated in the figure, $Z_{1e}$ increases as $\theta_1$ increases in contrast to $Z_{1o}$,

**TABLE 1. The sixteen impedance sets for the parametric analysis on the proposed balun.**

| Case I: $Z_S = 35–j10\ \Omega$ and $Z_L = 60+j10\ \Omega$ | | | | | | | | | |
|---|---|---|---|---|---|---|---|---|---|
| Set | A | B | C | D | Set | E | F | G | H |
| $Z_{1A}\ (\Omega)$ | 50 | 120 | 55 | 70 | $Z_{2A}\ (\Omega)$ | 50 | 80 | 70 | 40 |
| $Z_{1B}\ (\Omega)$ | 50 | 80 | 80 | 60 | $Z_{2B}\ (\Omega)$ | 50 | 100 | 90 | 55 |
| $Z_3\ (\Omega)$ | 60 | 65 | 68 | 62 | $Z_3\ (\Omega)$ | 60 | 65 | 62 | 66 |
| Case II: $Z_S = 40–j90\ \Omega$ and $Z_L = 70+j100\ \Omega$ | | | | | | | | | |
| Set | I | J | K | L | Set | M | N | O | P |
| $Z_{1A}\ (\Omega)$ | 50 | 120 | 55 | 70 | $Z_{2A}\ (\Omega)$ | 50 | 80 | 75 | 60 |
| $Z_{1B}\ (\Omega)$ | 50 | 80 | 80 | 60 | $Z_{2B}\ (\Omega)$ | 50 | 100 | 60 | 65 |
| $Z_3\ (\Omega)$ | 60 | 120 | 110 | 110 | $Z_3\ (\Omega)$ | 60 | 120 | 110 | 80 |

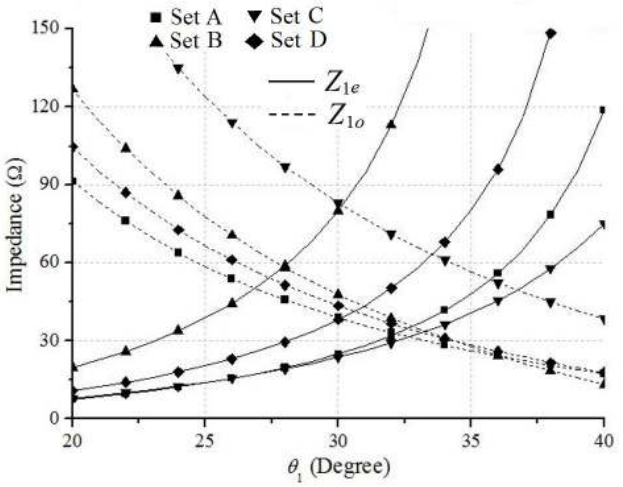


**FIGURE 6. The variations of $Z_{1e}$ and $Z_{1o}$ of the left DSCL subject to the changes in $\theta_1$ for Case I ($Z_S = 35 - j10\ \Omega$ and $Z_L = 60 + j10\ \Omega$).**

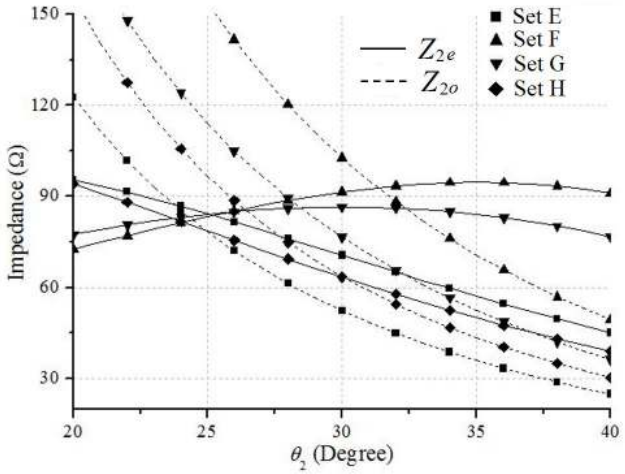


**FIGURE 7.** The variations of $Z_{2e}$ and $Z_{2o}$ of the right DSCL subject to the changes in $\theta_2$ for Case I ($Z_S = 35 - j10\ \Omega$ and $Z_L = 60 + j10\ \Omega$).

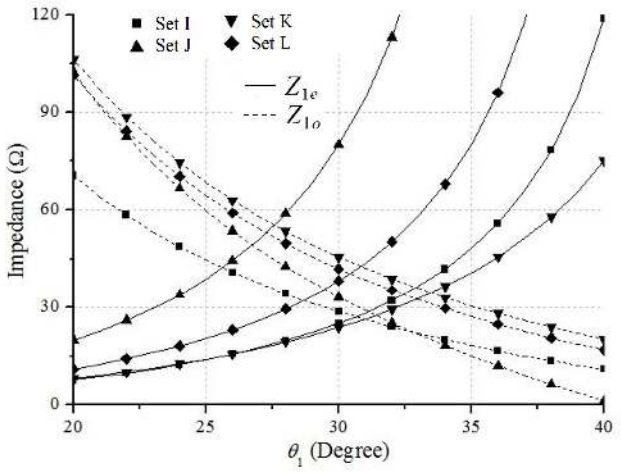


**FIGURE 8.** The variations of $Z_{1e}$ and $Z_{1o}$ subject to the changes in $\theta_1$ for Case II ($Z_S = 40 - j90\ \Omega$ and $Z_L = 70 + j100\ \Omega$).

which varies inversely. A larger $\theta_1$ would result in a higher impedance ratio of $Z_{1e}/Z_{1o}$, which would make the fabrication of coupled lines difficult. A criterion to follow is the value of $Z_{1e}/Z_{1o}$ less than 3. However, when $\theta_1$ is less than 27°, the coupled lines become impractical since the value of the corresponding $Z_{1e}$ is less than that of the paired $Z_{1o}$. Based on the comparisons made among Sets A–D, a larger $Z_{1A}$ would lead to a larger $Z_{1e}$; while a larger $Z_{1B}$ could result in a larger $Z_{1o}$. In summary, the impedance values specified in Set A and a value of 34° for $\theta_1$ are chosen to seek for the appropriate values for $Z_{1e}$ and $Z_{1o}$. The final selected values for $Z_{1e}$ and $Z_{1o}$ are 41.73 Ω and 31.34 Ω, respectively.

Fig 7 shows the variations of $Z_{2e}$ and $Z_{2o}$ of the right DSCL subject to the changes in $\theta_2$ for Case I. The impedance $Z_{2o}$ varies similarly as $Z_{1o}$ does in Fig. 6; however, $Z_{2e}$ changes differently from $Z_{1e}$ because of the existence of $R_o$, resulting in irregular curves. The rules to choose the appropriate values for $Z_{1e}$ and $Z_{1o}$ can also apply to the search for the suitable values for $Z_{2e}$ and $Z_{2o}$ by referring to Fig. 7, which suggests the impedance values described by Set F and a value of 36° for $\theta_2$. The appropriate values for $Z_{2e}$ and $Z_{2o}$ are 94.5 Ω and 54.69 Ω, respectively.

Fig. 8 shows the variations of $Z_{1e}$ and $Z_{1o}$ of the left DSCL subject to the changes in $\theta_1$ for Case II. The curves representing $Z_{1e}$ and $Z_{1o}$ for Case II are similar to their counterparts in Fig. 6 for Case I, but with lower impedance values compared to the values in Fig. 6. Therefore, the rules used for Case I can apply to Case II as well to choose the appropriate values for $Z_{1e}$ and $Z_{1o}$ by referring to the design curves in Fig. 8. Fig. 9 shows the variations of $Z_{2e}$ and $Z_{2o}$ versus the changes in $\theta_2$, in which both $Z_{2e}$ and $Z_{2o}$ increase tremendously as $\theta_2$ decreases, much faster than their counterparts do in Fig. 7. Since $Z_{2e}$ and $Z_{2o}$ of higher values may cause the same fabrication problem, a longer $\theta_2$ leading to lower even- and odd-mode impedances is preferred for this case. To transform complex impedances with a large reactance, an increase in $Z_3$ and a longer $\theta_2$ can help to bring $Z_{2e}$ and $Z_{2o}$ into the feasible range of the coupled line.

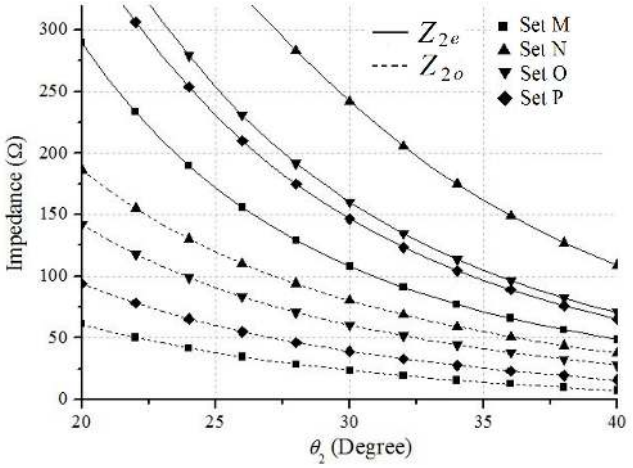


**FIGURE 9.** The variations of $Z_{2e}$ and $Z_{2o}$ subject to the changes in $\theta_2$ for Case II ($Z_S = 40 - j90\ \Omega$ and $Z_L = 70 + j100\ \Omega$).

To achieve the goals of transformation of complex impedances and high isolation, the right DSCL is loaded with an isolation resistor $R_o$. Fig. 10 shows the variations of $R_o$ subject to the changes in $\theta_2$ for both Cases I and II. The value of $R_o$ decreases as $\theta_2$ increases. The curves representing Case I vary more slowly than the ones representing Case II do. The values of $R_o$ for all the impedance sets are within the feasible range of 2–60 Ω for implementation. The utmost concern for the proposed design is the values of the even- and odd-mode impedances. As shown in Figs 6–10, there are multiple choices presented for their values, which is one of the advantages offered by this design.

## III. EXPERIMENTAL VERIFICATION AND DISCUSSION

The design procedure for the proposed design is summarized as follows.

1) Choose the impedance values from Sets A–P in Table 1 as the initial values for the design parameters of

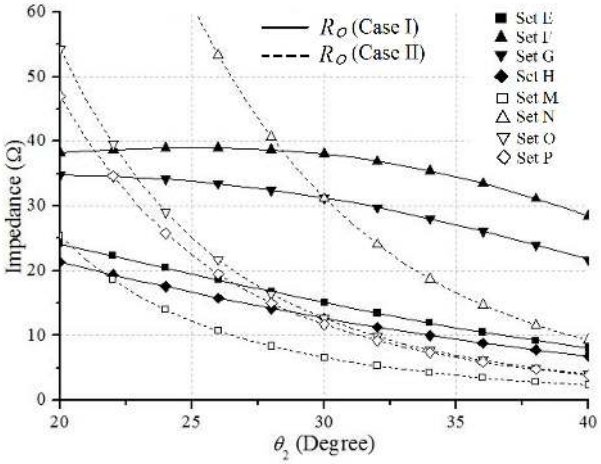


**FIGURE 10.** The variations of $R_o$ subject to the changes in $\theta_2$ for both Cases I and II.

**TABLE 2.** The design parameters of the proposed balun.

| $Z_{1A}$ | $Z_{1B}$ | $Z_{1e}$ | $Z_{1o}$ | $\theta_1$ | $Z_{2A}$ | $Z_{2B}$ |
|---|---|---|---|---|---|---|
| 50 Ω | 50 Ω | 41.73 Ω | 31.34 Ω | 34° | 80 Ω | 100 Ω |
| $Z_{2e}$ | $Z_{2o}$ | $\theta_2$ | $Z_3$ | $\theta_3$ | $R_o$ | |
| 94.5 Ω | 54.69 Ω | 36° | 62.7 Ω | 90° | 33.48 Ω | |

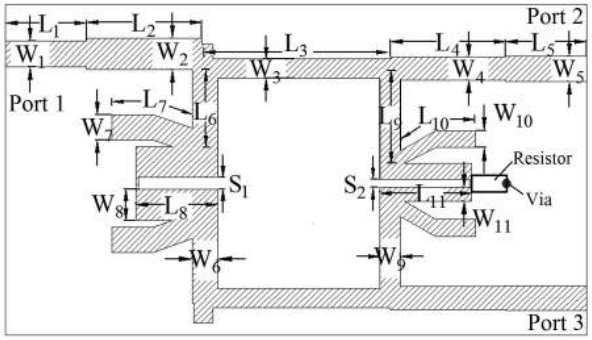


**FIGURE 11.** The circuit layout for the proposed balun.

the DSCLs with the given values for $Z_S$ and $Z_L$ and a fixed value of 90° for $\theta_3$.

2) The criterion for selecting appropriate even- and odd-mode impedances is the values of $Z_{1e}/Z_{1o}$ and $Z_{2e}/Z_{2o}$ less than 3.

3) Apply (5) and refer to Fig. 6 and Fig. 8 to determine the appropriate values for $Z_{1e}$, $Z_{1A}$, $Z_{1B}$, and $\theta_1$ of the left DSCL and $Z_3$.

4) Obtain the values of $Z_{2e}$,$R_o$, $Z_{2A}$, $Z_{2B}$, and $\theta_2$from (7), (8), Fig. 7, Fig. 9, and Fig. 10 for the right DSCL.

5) Apply (3b), (6), (9)–(11) and refer to Figs. 6–9 to determine the appropriate values for $Z_{1o}$ and $Z_{2o}$ of the DSCLs.

To validate the proposed design, a design example operating at 2.8 GHz and conducting impedance transformation defined by Case I is presented. The design parameters of the proposed design went through the optimization process

**TABLE 3.** The dimensions of the circuit from Fig. 11 (all in mm).

| $L_1$ | $L_2$ | $L_3$ | $L_4$ | $L_5$ | $L_6$ | $L_7$ | $L_8$ | $L_9$ | $L_{10}$ | $L_{11}$ | $S_1$ |
|---|---|---|---|---|---|---|---|---|---|---|---|
| 7 | 10 | 17 | 10 | 7 | 7.2 | 7.2 | 7.2 | 7.9 | 7.9 | 7.9 | 0.6 |
| $W_1$ | $W_2$ | $W_3$ | $W_4$ | $W_5$ | $W_6$ | $W_7$ | $W_8$ | $W_9$ | $W_{10}$ | $W_{11}$ | $S_2$ |
| 1.7 | 2.7 | 1.2 | 1.3 | 1.7 | 1.8 | 2.7 | 1.6 | 0.7 | 0.4 | 0.8 | 0.4 |

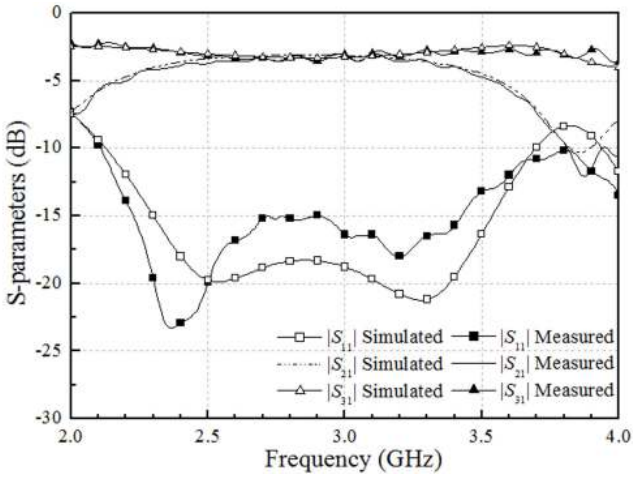


**FIGURE 12.** The comparison between the simulated and measured $|S_{11}|$, $|S_{21}|$, and $|S_{31}|$ of the proposed balun.

provided by the commercial EM simulator, HFSS, and their final values are tabulated in Table 2. A 33-Ω resistor is selected to improve output isolation and to contribute to transformation of complex impedances. The circuit was fabricated on a 0.762-mm-thick Arlon 25N substrate with a dielectric constant of 3.38 and a loss tangent of 0.0027, and its layout is displayed in Fig. 11. The dimensions of the circuit are listed in Table 3, where the same subscript is adopted for the symbols representing the width and the length of each transmission line.

To conduct standard measurements for the proposed design via a network analyzer, the inherent complex impedances at the input and output ports must be transformed to the 50-Ω system impedance. The following are the design formulas for the complex impedance transformer, which can convert a complex impedance $Z_1$ to $Z_2$ [19].

$$Z_1 = R_1 + jX_1, \tag{12a}$$

$$Z_2 = R_2 + jX_2, \tag{12b}$$

$$Z_T = \sqrt{\frac{R_1|Z_2|^2 - R_2|Z_1|^2}{R_2 - R_1}}, \tag{12c}$$

$$\theta_T = \tan^{-1}\left(\frac{Z_T(R_2 - R_1)}{R_2X_1 + R_1X_2}\right), \tag{12d}$$

where $Z_T$ and $\theta_T$ are the characteristic impedance and electrical length of the transformer, respectively. The input impedance of $35 - j10$ Ω requires a line of 37.64 Ω in impedance and 48.47° in length for the conversion. A line

**TABLE 4.** The comparisons on the performance of the proposed design and the baluns from published studies.

| Ref. | $f_0$ (GHz) | $\|S_{21}\|$ (dB) | $\|S_{31}\|$ (dB) | $\angle S_{31}-\angle S_{21}$ (°) | Isolation (dB) | Impedance transformation ($Z_L/Z_S$) Ω | Bandwidth (phase imbalance) | Bandwidth ($\|S_{11}\|$) | Bandwidth (amplitude imbalance) |
|---|---|---|---|---|---|---|---|---|---|
| [3] | 2 | –3.45 | –3.08 | –176.1 | –22.5 | 60+*j*10/35–*j*10 | 9.8% (±10°) | 9.8% (<–13 dB) | 9.8% (±1 dB) |
| [6] | 2.45 | –3.82 | –3.62 | 179.57 | No such function | No such function | Not provided | 20.41% (<–10 dB) | Not provided |
| [12] | 1.39 | –3.5 ~ –4 | –3.5 ~ –4 | –183 | No such function | No such function | Not provided | 96% (<–10 dB) | 96.9% (<1 dB) |
| [13] | 2.4 | –3.8 | –3.8 | 179 | –18 | No such function | 64% (±5°) | 64% (<–10 dB) | Not provided |
| [15] | 1.5 | –3.5 | –3.5 | –177.5 | No such function | No such function | Not provided | 83.3% (<–10 dB) | Not provided |
| [16] | 2.45 | –3.6 | –3.4 | 176 | No such function | No such function | 36.7% (±6°) | Not provided | 36.7% (< 0.5 dB) |
| **This work** | **2.8** | **–3.21** | **–3.28** | **180.2** | **–14.2** | **60+*j*10/35–*j*10** | **56% (±5°)** | **67.9% (<–10 dB)** | **35% (< 1 dB)** |

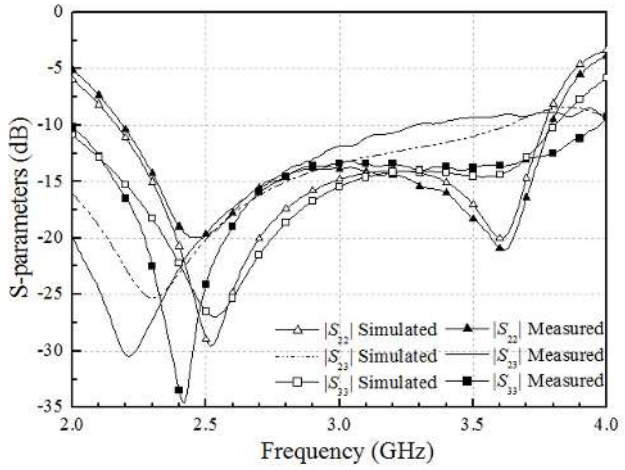


**FIGURE 13.** The comparison between the simulated and measured $|S_{22}|$, $|S_{23}|$, and $|S_{33}|$ of the proposed balun.

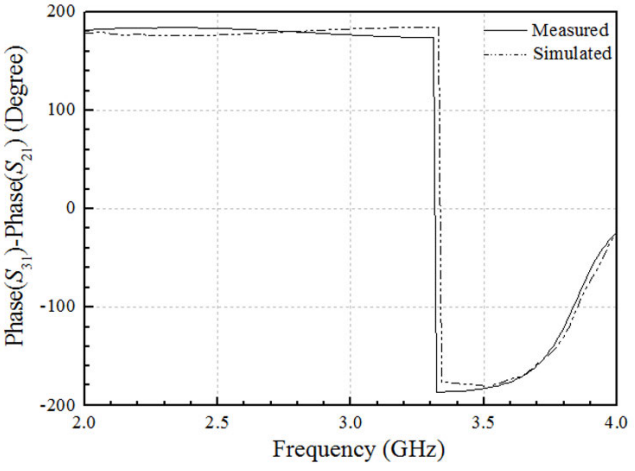


**FIGURE 14.** The comparison between the simulated and measured $\angle S_{31}-\angle S_{21}$

characterized by an impedance of 59.16 Ω and a length of 49.8° would serve to transform the load impedance of $60+j10$ Ω into $50-\Omega$ system impedance. These impedance transformers are included in Fig. 11 and directly connected to the input/output ports for measurements.

Fig. 12 shows the simulated and measured $|S_{11}|$, $|S_{21}|$, and $|S_{31}|$ of the proposed design. The transmission curves show great consistency between the simulation results and measurement data. The measured bandwidth under the criterion of $(|S_{31}|-|S_{21}|) < 1$ dB ranges from 2.34 to 3.34 GHz, which amounts to a fractional bandwidth of 35%. The values of $|S_{21}|$ and $|S_{31}|$ at 2.8 GHz are −3.21 and −3.28 dB, respectively. The measured bandwidth of $|S_{11}|$ less than −10 dB extends from 2.1 to 4 GHz, which is equivalent to a fractional bandwidth of 67.9%.

Fig. 13 shows that the measured return loss at the output ports match well with their simulated counterparts. The maximum value of the measured isolation is −30.5 dB and occurs at 2.2 GHz. The measured $|S_{11}|$ $|S_{22}|$, $|S_{33}|$, and $|S_{23}|$ are better than −14.2 dB, at 2.8 GHz, which indicates the performance of complex impedance transformation and high isolation.

Fig. 14 further compares the measured and simulated phase differences between the two output signals. As can be seen from the figure, the two curves are in great agreement throughout the entire frequency range of this study. The bandwidth of $\angle S_{31} - \angle S_{21}$ within the range of 180°±5° extends from 2.0 to 3.56 GHz, which is equal to a fractional bandwidth of 56%. The value of the phase difference at 2.8 GHz is 180.2°.

If all three conditions of $|S_{11}| < -10$ dB, $(\angle S_{31} - \angle S_{21}) < 180°\pm5°$, and $(|S_{31}| - |S_{21}|) < 1$ dB are satisfied simultaneously, then the operating bandwidth ranges from 2.34 to 3.34 GHz (or 35%), which is useful

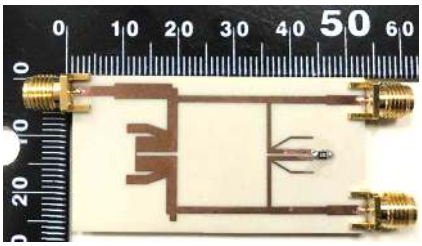

**FIGURE 15.** Photograph of the fabricated balun.

for wideband applications. Note that the measured results include the effect of the impedance transformation conducted at the input and output ports for measurements. The actual results would have been better without these impedance transformers.

The fabricated circuit of the proposed design is displayed in Fig. 15. The circuit exhibits a small size of $0.35\times0.78\ \lambda_g^2$ with the impedance transformers included for measurements, and $\lambda_g$ is the guided wavelength at 2.8 GHz. Table 4 compares the performance of the proposed design and the baluns from published studies. As indicated, this design demonstrates superior performance on transformation of complex impedances, high isolation, and wide bandwidth.

## IV. CONCLUSION

This paper presents a broadband balun with superior performance on complex impedance transformation and isolation. The proposed design is a 2.8-GHz balun constructed by DSCLs to achieve the goals of wide bandwidth, and transformation of complex source and load impedances. The differential characteristics are established by suppressing the even-mode operation, but exciting the odd-mode operation of a branch-line coupler. An isolation resistor is added to the DSCL between the output ports to improve isolation and to contribute to impedance transformation. A measured wide bandwidth of 35% is obtained under the criterions of $|S_{11}| < -10$ dB, $(\angle S_{31} - \angle S_{21}) < 180°\pm5°$, and $(|S_{31}| - |S_{21}|) < 1$ dB.

## REFERENCES

[1] M. J. Park and B. Lee, "Stubbed branch line balun," *IEEE Microw. Wireless Compon. Lett.*, vol. 17, no. 3, pp. 169–171, Mar. 2007.
[2] Y. Wu, L. Yao, W. Zhang, W. Wang, and Y. Liu, "A planar dual-band coupled-line balun with impedance transformation and high isolation," *IEEE Access*, vol. 4, pp. 9689–9701, 2016.
[3] W. Zhang, Y. Wu, Y. Liu, C. Yu, and W. Chen, "Compact coupled-line balun with complex impedances transformation and high isolation," *IET Microw., Antenna Propag.*, vol. 9, no. 14, pp. 1587–1594, Nov. 2015.
[4] M. Frank, M. Thorsell, and P. Enoksson, "Design equations for lumped element balun with inherent complex impedance transformation," *IEEE Trans. Microw. Theory Techn.*, vol. 65, no. 12, pp. 5162–5170, Dec. 2017.
[5] H. Zhu and A. M. Abbosh, "Modified wideband Marchand balun with tunable power division ratio and constant phase," *IEEE Microw. Wireless Compon. Lett.*, vol. 26, no. 5, pp. 319–321, May 2016.
[6] Y. Wang and J.-C. Lee, "A miniaturized Marchand balun model with short-end and capacitive feeding," *IEEE Access*, vol. 6, pp. 26653–26659, 2018.
[7] L.-P. Feng and L. Zhu, "Compact wideband filtering balun using stacked composite resonators," *IEEE Access*, vol. 6, pp. 34651–34658, 2018.
[8] J.-M. Yan, H.-Y. Zhou, and L.-Z. Cao, "A novel filtering balun and improvement of its isolation performance," *IEEE Microw. Wireless Compon. Lett.*, vol. 27, no. 12, pp. 1056–1058, Dec. 2017.
[9] J.-S. Lim, H.-S. Yang, Y.-T. Lee, S. Kim, K.-S. Seo, and S. Nam, "E-band Wilkinson balun using CPW MMIC technology," *Electron. Lett.*, vol. 40, no. 14, pp. 879–881, Jul. 2004.
[10] H.-R. Ahn and T. Itoh, "New isolation circuits of compact impedance-transforming 3-dB baluns for theoretically perfect isolation and matching," *IEEE Trans. Microw. Theory Techn.*, vol. 58, no. 12, pp. 3892–3902, Dec. 2010.
[11] D.-H. Kwon, "A wideband balun and vertical transition between conductor-backed CPW and parallel-strip transmission line," *IEEE Microw. Wireless Compon. Lett.*, vol. 16, no. 4, pp. 152–154, Apr. 2006.
[12] J. Shao, R. Zhou, C. Chen, X.-H. Wang, H. Kim, and H. Zhang, "Design of a wideband balun using parallel strips," *IEEE Microw. Wireless Compon. Lett.*, vol. 23, no. 3, pp. 125–127, Mar. 2013.
[13] Z.-Y. Zhang, Y.-X. Guo, L. C. Ong, and M. Y. W. Chia, "A new wide-band planar balun on a single-layer PCB," *IEEE Microw. Wireless Compon. Lett.*, vol. 15, no. 6, pp. 416–418, Jun. 2005.
[14] T. Canning, J. R. Powell, and S. C. Cripps, "Optimal design of broadband microwave baluns using single-layer planar circuit technology," *IEEE Trans. Microw. Theory Techn.*, vol. 62, no. 5, pp. 1183–1191, May 2014.
[15] H.-X. Xu, G.-M. Wang, X. Chen, and T.-P. Li, "Broadband balun using fully artificial fractal-shaped composite right/left handed transmission line," *IEEE Microw. Wireless Compon. Lett.*, vol. 22, no. 1, pp. 16–18, Jan. 2012.
[16] Y. Ye, L.-Y. Li, J.-Z. Gu, and X.-W. Sun, "A bandwidth improved broadband compact lumped-element balun with tail inductor," *IEEE Microw. Wireless Compon. Lett.*, vol. 23, no. 8, pp. 415–417, Aug. 2013.
[17] R. K. Barik, R. Rajender, and S. S. Karthikeyan, "A miniaturized wideband three-section branch-line hybrid with harmonic suppression using coupled line and open-ended stubs," *IEEE Microw. Wireless Compon. Lett.*, vol. 27, no. 12, pp. 1059–1061, Dec. 2017.
[18] H.-R. Ahn and B. Kim, "Toward integrated circuit size reduction," *IEEE Microw. Mag.*, vol. 9, no. 1, pp. 65–75, Feb. 2008.
[19] P. I. Day, "Transmission line transformation between arbitrary impedances using the Smith chart (letters)," *IEEE Trans. Microw. Theory Techn.*, vol. MTT-23, no. 9, pp. 772–773, Sep. 1975.

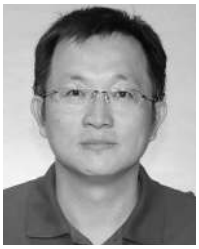

**ERIC S. LI** received the B.S. degree from Tamkang University, New Taipei City, Taiwan, in 1986, the M.S. degree in electrical engineering from the State University of New York, Stony Brook, NY, USA, in 1987, and the Ph.D. degree in electrical engineering from the University of Michigan, Ann Arbor, MI, USA, in 1998.

From 1988 to 1992 and from 1998 to 1999, he was in wireless industries as a Microwave Engineer participating in the designs of microwave circuits and antennas. From 1999 to 2006, he was a Faculty Member with the Department of Electrical Engineering, National Chi Nan University, Taiwan. Since 2006, he has been with the Department of Electronic Engineering, National Taipei University of Technology, Taiwan, where he is currently a Professor. His current research interests include microwave circuits, microwave calibration and measurement techniques, microwave and millimeter-wave polarimetric radar systems, and electromagnetic scattering.

**CHIN-TSE LIN** was born in Changhua, Taiwan. He received the B.S. degree in communication engineering from Feng Chia University, Taichung, Taiwan, in 2016, and the M.S. degree in electronic engineering from the National Taipei University of Technology, Taipei, Taiwan, in 2018.

His research interests include the designs of multifunctional microwave balun and microwave circuits.

**HUAYAN JIN** was born in Hangzhou, Zhejiang, China, in 1989. She received the B.S. degree in electronic engineering and the Ph.D. degree in electromagnetic field and microwave technology from the Nanjing University of Science and Technology (NUST), Nanjing, China, in 2011 and 2017, respectively. From August 2012 to January 2013, May 2013 to October 2013, and April 2014 to October 2014, she was an Exchange Student with the Chang Gung University, Taoyuan, Taiwan.

She is currently a Lecturer with the School of Electronics and Information, Hangzhou Dianzi University, Hangzhou, China. Her main research interests include millimeter-wave antennas, differential-fed antennas, and filtering antennas. She serves as a Reviewer for IEEE Access, *IET Electronics Letters*, and the *International Journal of Electronics*.

**KUO-SHENG CHIN** (S'05–M'06–SM'15) received the B.S. degree in electrical engineering from the Chung Cheng Institute of Technology, Taoyuan, Taiwan, in 1986, the M.S.E.E. degree from Syracuse University, Syracuse, NY, USA, in 1993, and the Ph.D. degree in communication engineering from National Chiao Tung University, Hsinchu, Taiwan, in 2005.

From 1986 to 2005, he was with the Chung Shan Institute of Science and Technology, Taoyuan, as a Research Assistant, becoming an Assistant Scientist, and then an Associate Scientist. He joined Chang Gung University, Taoyuan, as a Faculty Member, in 2006, where he is currently a Professor with the Department of Electronic Engineering. His current research interests include microwave and millimeter-wave circuits, low-temperature cofired ceramic circuits, array antennas, frequency-selective surfaces, radomes, and electromagnetic pulse research. He was a recipient of the Medal of Excellent Efficiency, the Order of Loyalty and Diligence, the Medal of Outstanding Staff, A Class, and the Medal of Army Achievement, A Class, all from the Ministry of National Defense, Taiwan, and the Outstanding Teaching Award of Chang Gung University, in 2014. He supervised a student team to win first place in the 2009 National Electromagnetism Application Innovation Competition, Taiwan. He was one of the recipients of the Best Paper Award of the International Conference on Electromagnetic Near Field Characterization and Imaging, in 2009, the Honorable Paper Award of the International High Speed Intelligent Communication Forum, in 2010, the Best Student Paper Award of the International Symposium on Next-Generation Electronics, in 2014, the Best Paper Award of the Taiwan Precision Engineering Workshop, in 2016, and the Best Student Paper Award of 2018 The 8th International Symposium on InfoComm and Mechatronics Technology in Biomedical and Healthcare Application. He serves as an Associate Editor of *Microwave and Optical Technology Letters*.